

Electronic and Magnetic Properties of the Interface between a doped cuprate $\text{Y}_{0.6}\text{Pr}_{0.4}\text{Ba}_2\text{Cu}_3\text{O}_7$ and a colossal-magnetoresistance manganite $\text{La}_{2/3}\text{Ca}_{1/3}\text{MnO}_3$

Jian Liu,¹ B. J. Kirby,² M. Kareev,¹ J. W. Freeland,³ H.-U. Habermeier,⁴ G. Cristiani,⁴ B. Keimer,⁴ and J. Chakhalian¹

¹*Department of Physics, University of Arkansas, Fayetteville, Arkansas 72701, USA*

²*Center for Neutron Research, National Institute of Standards and Technology, Gaithersburg, Maryland 20899, USA*

³*Advanced Photon Source, Argonne National Laboratory, Argonne, IL 60439, USA*

⁴*Max Plank Institute for Solid State Research, D-70569 Stuttgart, Germany*

(Dated: November 10, 2021)

The interfacial properties of $\text{Y}_{0.6}\text{Pr}_{0.4}\text{Ba}_2\text{Cu}_3\text{O}_7/\text{La}_{2/3}\text{Ca}_{1/3}\text{MnO}_3$ superlattices have been studied by resonant soft x-rays and diffuse scattered neutrons. Linearly polarized X-ray absorption at Cu L₃-edge reveals dramatic interfacial changes from the bulk including charge transfer between LCMO and YBCO and an orbital reconstruction in the interface CuO_2 plane. The similarities to the case of zero Pr-doping are due to the strongly hybridized covalent bond between Cu and Mn. However, reduced charge transfer and a more bulk-like interfacial orbital occupation are observed and related to the effect of Pr-doping. Neutron reflectometry measurements reveal a drastic increase in diffuse scattering with decreasing temperature, likely due to buckling caused by the structural phase transition of the SrTiO_3 substrate. We observe no evidence that this diffuse scattering is related to the superconducting transition.

PACS numbers:

Transition metal oxide (TMO) heterostructures have drawn enormous attention because of the strongly correlated nature of their electronic behaviors. The fine balance of the strong interactions between multiple degrees of freedom can be changed and even manipulated at the interfaces to create new phases that are not observed in the bulk materials. Heterostructures of high temperature superconducting cuprates and colossal magnetoresistance manganites are some of the most interesting oxide heterostructures due to their incompatible order parameters (i.e. half-metallic ferromagnetism (FM) vs superconductivity (SC)). In particular, the $\text{YBa}_2\text{Cu}_3\text{O}_7$ (YBCO) and $\text{La}_{2/3}\text{Ca}_{1/3}\text{MnO}_3$ (LCMO) heterostructures and superlattices are a representative of these systems which have been intensively studied. High-Tc SC was found to be suppressed by the presence of the LCMO layer and dependent on the thickness of the LCMO layer.¹ Metallicity in both LCMO and YBCO layers was also shown to be strongly suppressed with a large length scale.² Furthermore, a coupling of the superconducting layers was attributed to a long range proximity effect.³ On the other hand, X-ray Magnetic Circular Dichroism (XMCD) did not reveal significant change of moments on manganese while crossing the superconducting transition.⁴

Recently, special interest has been focused onto the microscopic picture of the YBCO/LCMO interface which also gives important insight into other TMO interfaces in general. Specifically, the splitting of the superlattice Bragg peak below the superconducting transition was observed by off-specular neutron reflectometry (NR).⁵ More surprisingly, XMCD at the Cu L-edge revealed that the interfacial CuO_2 plane of YBCO has a net magnetic moment with an unexpected antiferromagnetic coupling to Mn.⁵ This is explained by the interfacial orbital reconstruction (thereafter OR) observed by X-ray Linear

Dichroism (XLD) at the Cu L-edge.⁶ Namely, while the holes are constrained to Cu $d_{x^2-y^2}$ orbital in bulk, a significant number of holes occupy the $d_{3z^2-r^2}$ orbital at the interface. This is due to the strong covalent bond between Cu and Mn $d_{3z^2-r^2}$ orbitals causing the holes to move to the antibonding state during charge transfer.

A very interesting remaining question is what role superconductivity plays in YBCO/LCMO heterostructures. To address this question, one needs to study the case when SC is suppressed. One of the most interesting cases of suppressing High-Tc SC is doping with Pr in the $\text{RBa}_2\text{Cu}_3\text{O}_7$ (123) family (R= Y, Eu, Gd, etc.) because Pr is the only rare earth that maintains the crystal structure throughout the entire doping range and suppresses SC at the same time.^{7,8} For example, Pr substitutes Y in the case of YBCO, and SC is completely suppressed at as low as 50% doping ratio.⁹ These properties are well suited for oxide heterostructures since the oxygen stoichiometry can be maintained. In addition, a giant SC-induced modulation of the ferromagnetic magnetization from one LCMO layer to the next one in a Pr-doped YBCO/LCMO superlattice has been reported from NR lately.¹⁰ The suppressed SC was suggested to be an essential factor for the surprisingly large double-period modulation of the vertical magnetic profile, making Pr-doping especially interesting for the study of YBCO/LCMO heterostructures. Therefore, in this article, we report our study on (Y, Pr)BCO/LCMO superlattices which are similar to the previously studied YBCO/LCMO^{5,6} but with 40% Pr-doping to further suppress SC.

Superlattices with a nominal structure of $[\text{Y}_{0.6}\text{Pr}_{0.4}\text{Ba}_2\text{Cu}_3\text{O}_7 (100\text{\AA})/\text{La}_{2/3}\text{Ca}_{1/3}\text{MnO}_3 (100\text{\AA})]_5$ were grown on 0.5mm-thick, atomically flat (001) SrTiO_3 (STO) single crystal substrates by pulsed laser deposition with a KrF excimer Laser (248nm), the same

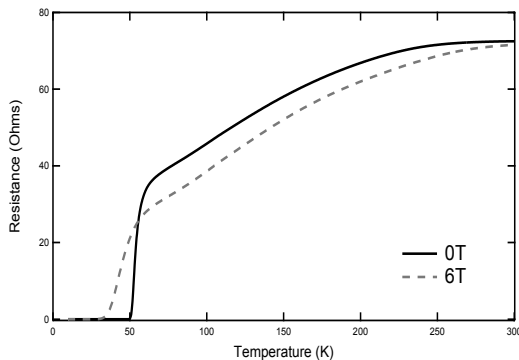


FIG. 1: Resistance vs temperature of [(Y,Pr)BCO (100Å)/LCMO (100Å)]₅ superlattices without magnetic field (solid curve) and with a magnetic field (dash curve) of 6T perpendicular to the film surface.

as previously studied YBCO/LCMO superlattices.⁵ The quality of the superlattices was checked by X-ray diffraction using Cu $K\alpha$ radiation (not shown). Only diffraction peaks due to (Y,Pr)BCO and LCMO are observed, indicating a pure single phase. Moreover, all (00 l) peaks are observed for both layers, confirming the high-quality c-axis oriented epitaxial growth. The corresponding (Y,Pr)BCO c-axis lattice parameter is around 11.66(3)Å which is consistent with the reported value of the orthorhombic $Y_{1-x}Pr_xBa_2Cu_3O_{7-\delta}$ structure.⁹

Temperature dependent resistance was measured in a PPMS (Quantum Design) with magnetic fields applied perpendicular to the film surface. The result shown in Fig. 1 reveals the well defined superconducting and magnetic behavior of the superlattice. At zero field, the superconducting transition T_{SC} ($R=0$) occurs around 50 K which is much lower than the case without Pr-doping. However, it is also slightly higher than the one corresponding to the nominal 40% Pr-doping ratio,⁹ indicating that the actual Pr concentration is appreciably lower. As a field of 6 T is applied, T_{SC} is suppressed to around 30 K, and the transition is significantly broadened accompanied by a positive magnetoresistance arising from vortex motion.¹¹ Compared to the case of YBCO/LCMO with the field in the ab-plane,⁶ the induced suppression and broadening by a field along c-axis are much more pronounced and characteristic of superconducting cuprates due to the two dimensional layered structure.¹² At higher temperature, negative magnetoresistance is observed resulting from the ferromagnetic state of LCMO. Such an observation confirms the high-quality growth of both (Y,Pr)BCO and LCMO layers as their characteristic bulk behaviors are held.

Linearly Polarized X-ray absorption experiments were performed at the 4-ID-C beamline¹³ of the Advanced Photon Source at Argonne National Laboratory. X-rays near Cu L_3 -edge with polarizations along the c-axis and in the ab-plane were used to obtain XLD. Absorption spectra were recorded simultaneously in both fluorescence yield (FY) mode and total electron yield (TEY)

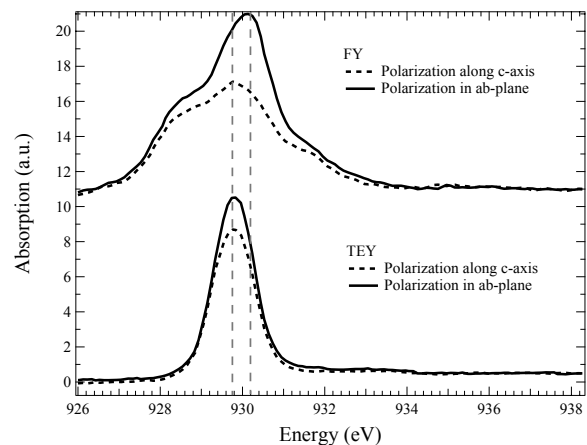


FIG. 2: Normalized X-ray absorption spectra at Cu L_3 -edge taken in (a) bulk-sensitive fluorescence mode and (B) interface-sensitive total electron yield mode. Dash lines are guides to eyes.

mode. These different modes provide different depth sensitivities: FY mode is sensitive to the bulk of the superlattice, while TEY mode probes the Cu state at the first interface covered by the top LCMO layer.⁶

Figure 2 shows the normalized spectra of the Cu L_3 -edge with in-plane and out-of-plane polarizations. Figure 2 (a) and (b) corresponds to the spectra in bulk-sensitive FY mode and interface-sensitive TEY mode, respectively. The FY data of both polarizations show a main peak at 930.1eV, a broad shoulder at lower energy and a relatively small shoulder at higher energy. The main peak corresponds to the $Cu\ 2p^63d^9 \rightarrow 2p^53d^{10}$ transition, while the small shoulder is due to $2p^63d^9L \rightarrow 2p^53d^{10}L$, where L denotes an oxygen ligand hole. Such a line shape of the Cu L_3 -edge absorption peak is the signature of the “Zhang-Rice (ZR) singlet state”.¹⁴ The shoulder on the left is due to the Pr M_5 -edge which partially overlaps with the Cu L_3 -edge and, therefore, was not resolved. This observation and the assignment above are consistent with other reported X-ray absorption data of Pr-doped cuprates.^{15,16,17} In spite of these common features of the FY data of both polarizations, it is clearly seen that the absorption of in-plane polarization is much more intense than that of polarization along c-axis. In particular, the difference reaches a maximum at the main peak but significantly decreases and almost disappears when passing the Pr M_5 -edge. Since, to our best knowledge, no XLD data at Pr M-edge is reported in literature for Pr-doped cuprates to compare with, based on the observed dichroism signal we conclude that there is no significant polarization dependence at the Pr M-edge. Consequently, one can see that the Cu L_3 -edge absorption of in-plane polarization is exceedingly stronger than that of polarization along c-axis by taking the Pr shoulder as the reference. Such an intense XLD of Cu L_3 -edge implies that the holes on the Cu d-shell predominantly occupy the planar $d_{x^2-y^2}$ orbital, which is also observed in all

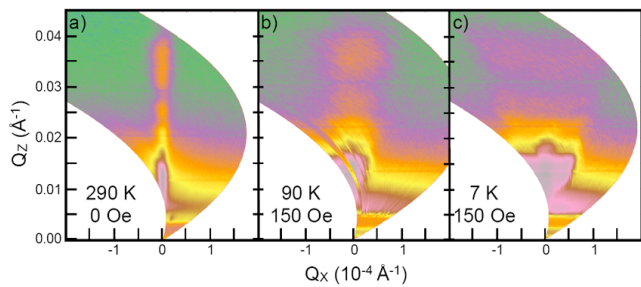


FIG. 3: (Color online) Off-specular neutron reflectivity taken at room temperature, 90K and 7K with a 15 mT cooling field applied parallel to the layers and perpendicular to the beam.

other high temperature superconductors.^{18,19} In contrast to the bulk, the picture at the interface shown by the interface-sensitive TEY data is dramatically different as can be seen in Fig. 2(b). First of all, the small shoulder due to $2p^63d^9L \rightarrow 2p^53d^{10}L$ transition in bulk is no longer present for either polarization, implying that the ZR state is destroyed at the interface. Surprisingly, the broad shoulder from Pr M_{5-} edge is also absent, by virtue of the electrostatic argument implying that it is more stable for Y ion to be located at the interfacial layer. More importantly, the position of the main absorption peak is shifted by $\sim 0.3\text{eV}$ towards lower energy, which is the sign of charge transfer across the interface between two materials with different work functions. Compared to the Cu L_3 -edge positions of other Cu valences, such a chemical shift corresponds to a charge transfer less than $0.2e$ per Cu ion.²⁰ Furthermore, the polarization dependence of the absorption at the interface is much weaker than in the bulk, which is the signature of the interfacial OR. The strong enhancement of the absorption intensity of polarization along c-axis illustrates that a large hole population resides on the $d_{3z^2-r^2}$ orbital. As mentioned earlier, an analogue of chemical shift and OR has also been observed at the interface between optimally doped YBCO and LCMO.⁶ Although SC is reduced by Pr-doping in the present case, the similar interfacial modification from the bulk is due to the strong hybridization nature of the covalent bonding between Cu and Mn.

However, there are still differences between these two cases. First, the amount of transferred charge is reduced in the present case given by the smaller shift of the absorption peak. Furthermore, the interfacial orbital occupation is more bulk-like evidenced by the relative intensity of the two polarizations. The explanation of these features is most likely related to the role played by Pr-doping. As is well known, at zero Pr-doping the ZR singlet band lies across the Fermi level in between the upper Hubbard band and the oxygen band. Although there is still controversy on how Pr-doping affects SC in the 123 family, it is widely accepted that, as the doping ratio increases, the so-called ‘‘Fehrenbacher-Rice’’ band emerges at the Fermi surface due to the strong hybridization be-

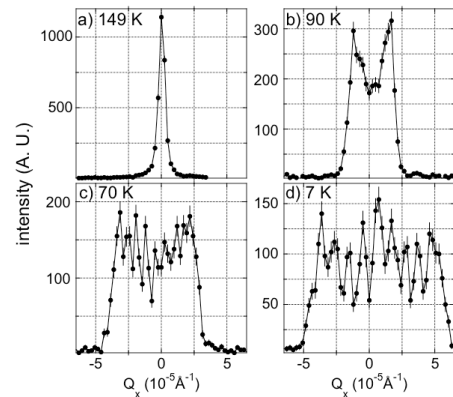


FIG. 4: Temperature-dependent unpolarized neutron transverse scans at $Q_z = 0.0139\text{\AA}^{-1}$ (right below the critical edge). Error bars correspond to $\pm\sigma$. Lines are guides to eye.

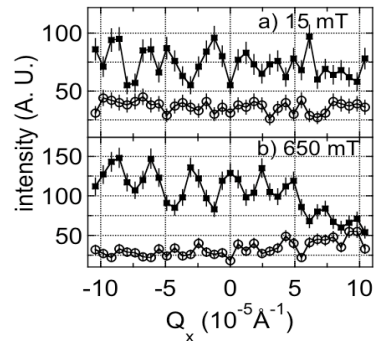


FIG. 5: Field-dependent polarized neutron transverse scans at $Q_z = 0.035\text{\AA}^{-1}$. Error bars correspond to $\pm\sigma$. Lines are guides to eye.

tween the O p state and the Pr $f_{z(x^2-y^2)}$ state.^{7,8,21} As a result, this emerging band removes the holes from the ZR band and consequently raises the Fermi level. Therefore, one would expect that the hole acquisition by LCMO at the interface is reduced and, hence, the partial occupancy of the Cu $d_{3z^2-r^2}$ orbital in the interfacial covalent bond decreases, as reflected in the experimental results.

Having obtained the effect of Pr-doping on the interfacial electronic structure, we also performed neutron reflectometry measurements, which are sensitive to the depth-dependent and planar composition (structural and magnetic) of thin-film multilayers.^{23,24} This was for comparison to previous NR studies on YBCO/LCMO multilayers grown on STO which exhibited interesting oscillatory diffuse scattering as SC sets in⁵ below the STO cubic-to-tetragonal phase transition at $T_{STO} = 105\text{ K}$.²² NR measurements were performed at the NIST Center for Neutron Research, using the AND/R and NG-1 reflectometers.^{25,26} For all measurements, the sample was mounted using a flexible aluminum backing (to minimize stress), and was cooled from room temperature to 150 K in zero field, and then further cooled to 7 K in the presence of an applied magnetic field. Figure 3 shows un-

polarized neutron scattering reciprocal space maps measured by a position sensitive detector. Scattering along the z -component of wavevector transfer (Q_z) (specular scattering) originates from structural and magnetic features along the growth direction of the sample, while scattering along the Q_x axis (diffuse scattering) corresponds to in-plane features. At room temperature (3a), purely nuclear scattering is observed along the specular ridge ($Q_x=0$) and a superlattice Bragg peak is clearly observable ($Q_z \approx 0.035 \text{ \AA}^{-1}$). As the temperature is reduced below T_{STO} (3b-c), the specular ridge dramatically diffuses out along the Q_x direction- indicating significantly increased in-plane inhomogeneity. To identify the nature of this planar inhomogeneity, a series of higher resolution “transverse scans” (fixed Q_z) were taken using a 3He pencil detector. Figure 4 shows temperature-dependent, unpolarized beam transverse scans taken at $Q_z = 0.0139 \text{ \AA}^{-1}$ (just below the critical edge) in a 650 mT field. Below T_{STO} , diffuse scattering is again observed, but in this case pronounced oscillations in Q_x are clearly resolvable.²⁷ Qualitatively similar results were obtained at a 15 mT field (not shown). Figures 4b-d show that this oscillatory diffuse scattering is present both above and below T_{SC} , indicating that the onset of SC plays no role in its origin. Figure 5 shows the results of polarized beam transverse scans taken at the 1st superlattice Bragg position after cooling in 650 mT (5a) and 15 mT (5b). Non spin-flip scattering of spin-up or spin-down neutrons is evident (no significant spin-flip scattering could be detected). While the overall spin-splitting (related to the total sample magnetization^{23,24}) increases with increasing field, the oscillatory nature of the diffuse scattering is similar for both fields - strongly suggesting that it is not a magnetic effect. Instead, it is exceedingly

likely that the observed in-plane modulation described above is primarily due to the STO structural phase transition which is associated with crystallographic twinning and surface buckling.^{5,22} Specifically, we expect that the superlattice film becomes faceted below T_{STO} , causing the specular reflection to split into multiple reflections, similar to the observation by Hoppler et al. (Ref. 10,28). A SC-induced period doubling of the magnetization profile along the c -axis was not observed in our study, perhaps as a consequence of the previously noted¹⁰ sensitivity of this phenomenon to external boundary conditions.

In conclusion, we have grown high-quality $\text{Y}_{0.6}\text{Pr}_{0.4}\text{Ba}_2\text{Cu}_3\text{O}_7/\text{La}_{2/3}\text{Ca}_{1/3}\text{MnO}_3$ superlattices. The interfacial reconstruction was studied by linearly polarized X-ray absorption at the Cu L_3 -edge. Similar to the interface between optimally doped YBCO and LCMO, we observed dramatic modifications including charge transfer and OR at the interfacial CuO_2 plane of Pr-doped YBCO due to the strongly hybridized covalent bond between Cu and Mn. However, differences such as reduced charge transfer and more bulk-like orbital occupation were also found. This is presumably related to the Pr-doping which removes holes from the ZR state and suppresses SC. Neutron reflectivity data revealed temperature-dependent, oscillatory diffuse scattering, indicative of a significant in-plane modulation, which can be attributed to buckling of the superlattice film due to the structural phase transition of the STO substrate.

Acknowledgments J.C. was supported by DOD-ARO under the Contract No. 0402-17291 and NSF Contract No. DMR-0747808. Work at the Advanced Photon Source, Argonne is supported by the U.S. Department of Energy, Office of Science under Contract No. DEAC02-06CH11357.

-
- ¹ Z. Sefrioui *et al.*, Phys. Rev. B **67**, 214511 (2003).
² T. Holden *et al.*, Phys. Rev. B **69**, 064505 (2004).
³ V. Pena *et al.*, Phys. Rev. B **69**, 224502 (2004).
⁴ J. W. Freeland *et al.*, Appl. Phys. Lett. **90**, 242502 (2007).
⁵ J. Chakhalian *et al.*, Nature Physics **2**, 244 (2006).
⁶ J. Chakhalian *et al.*, Science **318**, 1114 (2007).
⁷ R. Fehrenbacher and T.M. Rice, Phys. Rev. Lett. **70**, 3471 (1993); A.I. Liechtenstein and I.I. Mazin, *ibid.* **74**, 1000 (1995).
⁸ I.I. Mazin and A.I. Liechtenstein, Phys. Rev. B **57**, 150 (1998).
⁹ J. L. Peng *et al.*, Phys. Rev. B **40**, 4517 (1989).
¹⁰ J. Hoppler *et al.*, Nature Materials **8**, 315 (2009).
¹¹ T. T. M. Palstra *et al.*, Phys. Rev. Lett. **61**, 1662 (1988).
¹² For example, M. Oda *et al.*, Phys. Rev. B **38**, 252 (1988).
¹³ J. W. Freeland *et al.*, Rev. Sci. Instrum. **73**, 1408 (2001).
¹⁴ F. C. Zhang and T. M. Rice, Phys. Rev. B **37**, 3759 (1988).
¹⁵ U. Neukirch *et al.*, Europhys. Lett. **5**, 567 (1988).
¹⁶ J.M. Chen *et al.*, Chem. Phys. Lett. **294**, 209 (1998).
¹⁷ J. M. Chen *et al.*, Phys. Rev. B **55**, 14586 (1997).
¹⁸ N. Nücker *et al.*, Phys. Rev. B **51**, 8529 (1995).
¹⁹ C. T. Chen *et al.*, Phys. Rev. Lett. **66**, 104 (1991).
²⁰ F. M. F. de Groot, J. Electron Spectrosc. Relat. Phenom. **67**, 529 (1994).
²¹ M. Merz *et al.*, Phys. Rev. B **55**, 9160 (1997).
²² V. K. Vlasko-Vlasov *et al.*, Phys. Rev. Lett. **84**, 2239 (2000).
²³ C. F. Majkrzak, K. V. O'Donovan, and N. F. Berk, in *Neutron Scattering From Magnetic Materials*, edited by T. K. Chatterji (Elsevier Science, Amsterdam, 2005).
²⁴ Hartmut Zabel, Katharina Theis-Bröhl, and Boris P. Toperverg, in *Handbook of Magnetism and Advanced Magnetic Materials*, edited by Helmut Kronmüller and Stuart Parkin (Wiley, 2007), Vol. 3
²⁵ J. A. Dura *et al.*, Rev. Sci. Instrum. **77**, 074301 (2006).
²⁶ See <http://www.ncnr.nist.gov/instruments/andr> and <http://www.ncnr.nist.gov/instruments/ng1refl>
²⁷ That Q_x oscillations are distinguishable in Fig. 5, but not in Fig. 4 may be due to the better resolution of the pencil detector as compared to the position sensitive detector. However, variations in external stress due to small differences in sample mounting for the two sets of measurements may also contribute to differences between Fig. 4 and 5.
²⁸ J. Hoppler *et al.*, Phys. Rev. B **78**, 134111 (2008).